Different Conformational Switches Underlie the Calmodulin-Dependent Modulation of Calcium Pumps and Channels†

Curt B. Boschek, Hongye Sun,‡ Diana J. Bigelow, and Thomas C. Squier*

Cell Biology and Biochemistry Group, Biological Sciences Division, Pacific Northwest National Laboratory, Richland, Washington 99352

Received October 3, 2007; Revised Manuscript Received November 28, 2007

ABSTRACT: We have used fluorescence spectroscopy to investigate the structure of calmodulin (CaM) bound with CaM-binding sequences of either the plasma membrane Ca-ATPase or the skeletal muscle ryanodine receptor (RyR1) calcium release channel. Following derivatization with *N*-(1-pyrene)maleimide at engineered sites (T34C and T110C) within the N- and C-domains of CaM, contact interactions between these opposing domains of CaM resulted in excimer fluorescence that permits us to monitor conformational states of bound CaM. Complementary measurements take advantage of the unique conserved Trp within CaM-binding sequences that functions as a hydrophobic anchor in CaM binding and permits measurements of both a local and global peptide structure. We find that CaM binds with high affinity in a collapsed structure to the CaM-binding sequences of both the Ca-ATPase and RyR1, resulting in excimer formation that is indicative of contact interactions between the N- and the C-domains of CaM in complex with these CaM-binding peptides. There is a 4-fold larger amount of excimer formation for CaM bound to the CaM-binding sequence of the Ca-ATPase in comparison to RyR1, indicating a closer structural coupling between CaM domains in this complex. Prior to CaM association, the CaM-binding sequences of the Ca-ATPase and RyR1 are conformationally disordered. Upon CaM association, the CaM-binding sequence of the Ca-ATPase assumes a highly ordered structure. In comparison, the CaM-binding sequence of RyR1 remains conformationally disordered irrespective of CaM binding. These results suggest an important role for interdomain contact interactions between the opposing domains of CaM in stabilizing the structure of the peptide complex. The substantially different structural responses associated with CaM binding to Ca-ATPase and RyR1 indicates a plasticity in their respective binding mechanisms that accomplishes different physical mechanisms of allosteric regulation, involving either the dissociation of a C-terminal regulatory domain necessary for pump activation or the modulation of intersubunit interactions to diminish RyR1 channel activity.

Calmodulin (CaM)[1] functions as a central regulator of cellular metabolism in response to changes in cellular calcium levels (*1*). Calcium-activated CaM contains two high-affinity binding domains connected by a flexible interdomain sequence that permits its high-affinity association with more than 50 different target proteins with highly variable sequences (http://calcium.uhnres.utoronto.ca/ctdb/ctdb/browse.html) (*1*, *2*). The structural basis for this plasticity is a central question for understanding cellular responses to differences in calcium signaling. A useful experimental tool in this regard has been the in vitro use of peptides corresponding to the CaM-binding sequences of CaM-dependent target proteins. To date, 20 structures of CaM bound to different target proteins have been solved; these include apo-CaM (two structures), partially calcium-activated CaM (two structures), and fully activated Ca_4-CaM (16 structures) that highlight different modes of binding that affect target protein activation (see Figure S1 in the Supporting Information) (http://www.rcsb.org/pdb/). Plasticity in the binding mechanism is especially apparent in the structures with calcium-activated CaM bound, where variations are apparent in both the orientation and the spatial separation between the opposing domains of the bound CaM.

† This work was supported by Grant AG12993 from the National Institutes of Health. Pacific Northwest National Laboratory is operated for the United States Department of Energy by Battelle Memorial Institute under Contract DE-AC06-76RLO 1830.

* Corresponding author. Tel.: (509) 376-2218. Fax: (509) 376-6767. E-mail: thomas.squier@pnl.gov.

‡ Present Address: Applied Biosystems, 850 Lincoln Centre Dr., Foster City, CA 94404.

[1] Abbreviations: AEDANS, 5((((acetyl)amino)ethyl)amino)naphthalene-1-sulfonic acid; β-ME, 2-mercaptoethanol; CaM, calmodulin; C28W, CaM-binding sequence of the plasma membrane Ca-ATPase corresponding to residues L^{1100}RRGQILWFRGLNRIQTQIRVVNAFRSSS; C28W*, L^{1100}RRGQILWFRGLNRIQTQIRC*VNAFRSSS, where C* contains a covalently bound AEDANS; DTT, dithiothreitol; EGTA, glcol-bis(2-aminoethylether)-*N*,*N*,*N*′,*N*′-tetraacetic acid; HEPES, *N*-(2-hydroxyethyl)piperazine-*N*′-(2-ethanesulfonic acid); FRET, fluorescence resonance energy transfer; MLCK peptide, CaM-binding sequence of skeletal myosin light chain kinase corresponding to residues K^{577}-RRWKKNFIAVSAANRFKKISSSGAL^{602}; MS, mass spectrometry; P, steady-state polarization; Py, pyrene; Py_2-CaM, T34C,T110C-CaM labeled at both introduced cysteines with *N*-(1-pyrene)maleimide; RyRp, CaM-binding sequence of RyR1 corresponding to residues K^{3614}-SKKAVWHKLLSKQRRRAVVACFRMTPLYNK; SDS-PAGE, sodium dodecyl sulfate-polyacrylamide gel electrophoresis; TCEP, tris(carboxyethyl)phosphine; RyRp*, K^{3614}SKKAVWHKLLSKQRRRAVVACFRMTPLYNK*, where K* contains a covalently bound 5-dimethylaminonaphthalene-1-sulfonyl (dansyl) moiety.

10.1021/bi701987n CCC: $40.75
Published on Web 01/18/2008

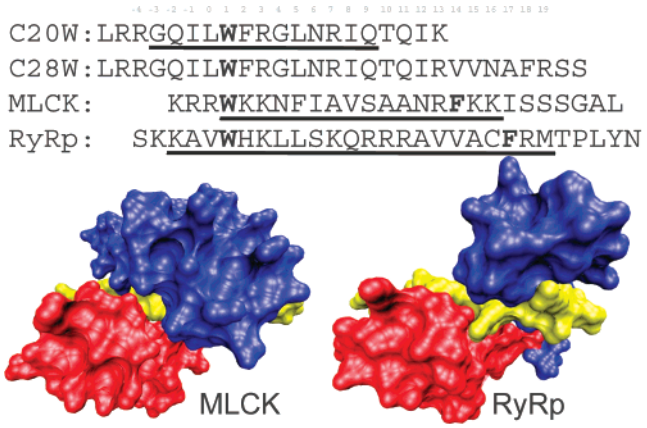

FIGURE 1: CaM-binding sequences and structures: CaM-binding sequences (top) of the plasma membrane Ca-ATPase (C20W or C28W), skeletal myosin light chain kinase (MLCK), and the ryanodine receptor calcium release channel (RyRp) and high-resolution structures (bottom) of CaM in association with MLCK and RyRp. Helical portions of peptides in association with CaM are underlined, as identified in respective structures 1cff, 2bbm, and 2bcx (*7*, *8*, *10*); numbers define spacing between hydrophobic anchors associated with CaM binding for the C-domain (i.e., Trp^{1}) and N-domain of either MLCK peptide (i.e., Phe^{14}) or RyRp (Phe^{17}). Models of 3-D structures were generated with VMD version 1.8.6 (*50*) and rendered with POV-ray version 3.5 (www.povray.org), where the CaM-binding sequence is in yellow and the C- and N-domains of CaM are, respectively, shown in red and blue.

The validity of these peptide-CaM structures is evidenced by the identical structures observed for CaM bound to (i) the intact protein and (ii) peptides corresponding to the CaM-binding sequence of CaM-dependent protein kinase I (CaMKI) and the plasma membrane Ca-ATPase (*3*−*5*). Likewise, calcium-dependent changes in the association between CaM and the high-affinity CaM-binding sequence in the ryanodine receptor calcium release channel (RyR1) match the calcium dependence of the intact RyR1 channel function (*6*). These results imply that CaM-induced structural rearrangements within the CaM-binding sequence of these target proteins can provide important information regarding the functional regulation of CaM-dependent enzymes.

The helical content of the CaM-binding sequences of Ca-ATPase and RyR1 in complex with CaM are very different and represent extreme examples within the current family of high-resolution structures. Aspects of the structural consequences of differences in CaM-binding sequences are apparent from a comparison of CaM bound to either Ca-ATPase or RyR1. The opposing domains of CaM bound to the CaM-binding site of the Ca-ATPase together form a rigid complex similar to that associated with skeletal MLCK (*4*, *5*), whose high-resolution structure showing both domains of CaM bound has been solved (*7*) (Figure 1). In comparison, the N- and C-domains of CaM remain widely separated upon association with the CaM-binding sequence of RyR1, resulting in some flexibility in the independent motions of the individual domains of CaM that is not expected from the high-resolution crystal structure (*8*). These results suggest that interdomain interactions between the opposing domains of CaM provide a significant contribution to the stabilization of the structure of the CaM-binding sequence. Differences in interdomain interactions of CaM bound to different target proteins may explain differences in the functional regulation of Ca-ATPase and RyR1.

We used fluorescence spectroscopy to investigate the structural coupling between the N- and the C-domains of CaM bound to the CaM-binding sequences of Ca-ATPase and RyR1 and the relationship to the structure and dyanamics of the CaM-binding sequence. The spatial separation between the N- and the C-domains of CaM was assessed through the measurement of excimer formation following the site-specific derivatization of CaM with *N*-(1-pyrene)maleimides at engineered sites in both the N- and the C-domains of CaM (*9*). We have previously demonstrated that pyrene labeling at these sites does not perturb calcium binding or interactions with target proteins, consistent with high-resolution structures showing that these labeling sites are distant from binding interfaces between CaM and CaM-binding sequences of target proteins (*6*, *9*). To examine the structures of the CaM-binding sequences, we took advantage of the unique Trp that functions as a hydrophobic anchor in CaM binding, which permits measurements of the rotational dynamics of the peptide complex. Following introduction of a chromophore that acts as a fluorescence resonance energy transfer (FRET) acceptor within the CaM-binding sequence, frequency-domain lifetime measurements allowed a determination of the average structure and associated conformational heterogeneity of both C28W and RyRp. We find that while CaM binds with high affinity and in a collapsed structure to both C28W and RyRp, there is a substantially closer association between the opposing domains of CaM bound to C28W in comparison to RyRp. Upon CaM association, the C28W peptide assumes a highly compact and ordered structure. In contrast, RyRp retains some disorder when CaM is bound. These results suggest an important role for interdomain contact interactions between the opposing domains of CaM in stabilizing a coil-to-helix structural transition associated with the dissociation of the regulatory domain of the Ca-ATPase.

EXPERIMENTAL PROCEDURES

Materials. HPLC-purified peptides (>95%) corresponding to the CaM-binding sequence of RyR1 (K^{3614}SKKAVWHKLLSKQRRRAVVACFRMTPLYNK or RyRp), the plasma membrane Ca-ATPase (L^{1100}RRGQILWFRGLNRIQTQIRVVNAFRSSC or C28W), and skeletal myosin light chain kinase (K^{577}RRWKKNFIAVSAANRFKKISSSGAL or M13) were obtained from either SynPep (Dublin, CA), Quality Control Company (Hopkinton, MA), or Anaspec Labs (San Jose, CA). Two additional peptide analogues of RyRp and C28W were made in which a FRET acceptor to Trp was incorporated into the peptide during synthesis. These peptides incorporated either a lysine covalently bound to 5-dimethylaminonaphthalene-1-sulfonyl introduced at position 3644 (RyRp*) or a cysteine covalently bound to 5((((acetyl)amino)ethyl)amino)naphthalene-1-sulfonic acid introduced at position 1120 (C28W*). In both cases, sites for the incorporation of the FRET acceptor were chosen based on the respective crystal structures to be five amino acids toward the C-terminus of the identified helical structure of the CaM-binding sequence suggested to be associated with enzyme functional regulation for Ca-ATPase (1cff) or RyR1 (2bcx) (*8*, *10*) (Figure 1).

Expression and Purification of CaM. Plasmids encoding wild-type and a mutant CaM containing two cysteines (i.e., T34C T110C) were expressed in a BL21 (DE3) *Escherichia*

coli strain, as previously described (*9*). CaM was purified by chromatography on phenyl sepharose CL-4B (Pharmacia, Piscataway, NJ), and the protein concentration was measured using a micro BCA assay reagent kit (Pierce, Rockford, IL) using desalted wild-type CaM as the standard ($\epsilon_{277} = 3029$ M^{-1} cm^{-1}) (*11*).

Covalent Labeling of CaM with Pyrene. CaM was specifically labeled with *N*-(1-pyrene)maleimide in either domain, as previously described (*9*). Briefly, CaM mutant T34C, T110C in 10 mM HEPES (pH 7.8) was reduced with 0.25 μM tris(carboxyethyl)phosphine (TCEP) prior to the addition of a 20-fold molar excess of *N*-(1-pyrene)maleimide. After incubation for 2 h, excess dye was removed using a Sephadex G25 size-exclusion column. The stoichiometry of bound pyrene was measured using the extinction coefficient $\epsilon_{340} =$ 40 000 M^{-1} cm^{-1} (*12*), where 2.2 ± 0.3 mol of *N*-(1-pyrene)-maleimide binds per mol of CaM (*9*).

Fluorescence Measurements. Steady-state fluorescence spectra were acquired at 25 °C using a FluoroLog2 (Edison, NJ) instrument at 1 nm resolution with both excitation and emission slits set at 5 nm with an integration time of 0.1 s for spectra. Frequency-domain lifetime and anisotropy measurements involved the tripled output (297 nm) of a Ti-sapphire laser (Coherent, Santa Clara, CA, Mira 900) tuned to 891 nm, whose frequency was reduced to 5 MHz using a Coherent pulse picker (model 9200) to excite tryptophan. The fluorescence lifetime or anisotropy was measured using an ISS-K2 fluorometer (Urbana−Champaign, IL). The emitted fluorescence was, respectively, detected subsequent to an interference filter with a 10 band-pass centered at either 340 nm (C28W) or 350 nm (RyRp).

Analysis of Frequency-Domain Data. The time-dependent fluorescence decay, $I(t)$, was fit to a sum of exponentials, where the mean lifetime ($\bar{\tau}$) is

$$\bar{\tau} = \sum_{i=1}^{n} \alpha_i \tau_i \tag{1}$$

where α_i are the preexponential factors, τ_i are the excited-state decay times, and n is the number of exponential conponents required to describe the decay. Nonlinear least-squares fits to the data involved standard algorithms, and the goodness of fit was determined by minimizing the χ^2_R (the *F*-statistic) (*13*).

Determination of Conformational Heterogeneity Using FRET. A Gaussian distribution of donor−acceptor separations, $P(r)$, representing the conformational heterogeneity associated with polymeric structures can be measured from the frequency dependence of the intensity decay (*14*)

$$P(r) = \frac{1}{\sigma\sqrt{2\pi}} \exp\left[-0.5\left(\frac{r - R_{av}}{\sigma}\right)\right] \tag{2}$$

where R_{av} is the average distance, and σ is the standard deviation of the distribution. The width of the distribution is reported as the full-width at half-maximum (half-width, hw), which is given by hw = 2.354σ.

Decays of Fluorescence Anisotropy. Time-resolved anisotropies were measured at discrete frequencies ω using the phase angle difference (Δ_ω) and ratio of modulation amplitudes (Λ_ω) between the parallel and the perpendicular components of the emission, where $\Delta_\omega = (\varphi_\perp - \varphi_{||})$ and $\Lambda_\omega = m_{||}/m_\perp$. The modulated anisotropy is $(r_\omega) = (\Lambda_\omega - 1)/(\Lambda_\omega + 2)$], as previously discussed (*13*). The parameters describing the anisotropy decay were obtained from a least-squares fit to a multiexponential model

$$r(t) = r_o \sum_{i=1}^{n} g_i \, e^{-t/\phi_i} \tag{3}$$

where r_o is the limiting anisotropy in the absence of rotational diffusion, φ_i are the rotational correlation times, $r_o g_i$ are the amplitudes of the total anisotropy loss associated with each rotational correlation time, and n is the total number of components associated with the anisotropy decay. The goodness-of-fit was determined through a comparison of the deviations between the measured and the calculated values. Errors in Δ_ω and Λ_ω were assumed to be 0.2 and 0.02, respectively.

RESULTS

High-Affinity Binding of N- and C-Domains of CaM to Target Peptides. To assess possible differences in binding mechanisms, spatial arrangements were monitored for the N- and C-domains of CaM in association with the CaM-binding sequences of the plasma membrane Ca-ATPase and the RyR1 calcium release channel using fluorescence changes measured upon binding of pyrene-labeled CaM (Py_2-CaM) to peptides C28W and RyRp (Figures 1 and 2). For these measurements, CaM was engineered to contain two cysteines (T34C and T110C) located at surface exposed positions distant from binding interfaces between CaM and CaM-binding sequences of target proteins (*6*, *9*). Following derivatization with *N*-(1-pyrene)maleimide at engineered sites T34C and T110C within the N- and C-domains of CaM, contact interactions were measured from the formation of excited-state dimer (excimer) complexes as assessed by the diagnostic appearance of a fluorescence peak near 480 nm (*9*, *15*).

In the absence of a target peptide, there is little or no excimer fluorescence for calcium-activated Py_2-CaM, consistent with prior suggestions that calcium activation stabilizes an extended structure of CaM (*16*, *17*) (Figure 2A). On the other hand, the addition of either C28W or RyRp peptides results in significant excimer fluorescence, indicative of contact interactions between the N- and the C-domains of Py_2-CaM (Figure 2). In comparison, Py_2-CaM binding to the CaM-binding sequence of skeletal myosin light chain kinase (MLCK) results in an excimer fluorescence intensity that is virtually identical to that observed with the CaM-binding sequence of the Ca-ATPase, suggesting that the C28W-CaM complex adopts a structure similar to that illustrated by the high-resolution crystal structure available for CaM bound to the MLCK CaM-binding sequence (*7*). In this latter structure, CaM wraps around the target peptide forming extensive van der Waals contact interactions and with opposing domains of CaM coming into close juxtaposition.

Maximal excimer formation is observed near an equimolar ratio of added CaM-binding peptide to Py_2-CaM (Figure 2B). These results indicate an equimolar binding stoichiometry of the complex, ensuring that the observed excimer formation is the result of interdomain interactions in CaM. Half-

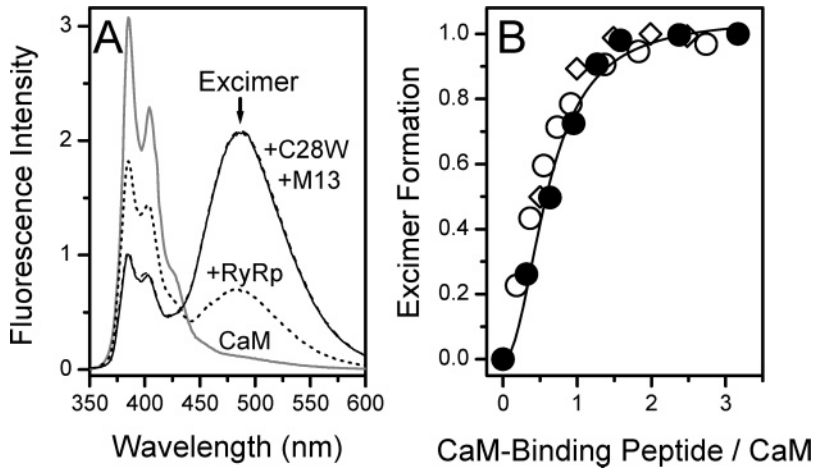

FIGURE 2: High-affinity association between opposing domains of CaM and target peptides. Emission spectra (A) and binding isotherms (B) for Py_2-CaM (100 nM) alone (solid gray line) and in the presence of peptides corresponding to the CaM-binding sequences of RyR1 (dotted line; ○), the Ca-ATPase (solid black line; ●), or MLCK (dashed line; ◇), where spectra (A) were obtained in the presence of 260 nM CaM-binding peptides. Experimental conditions involved 50 mM MOPS (pH 7.0), 0.1 M KCl, 1 mM $MgCl_2$, 1 mM EGTA, and 1.7 mM $CaCl_2$ (700 μM free calcium) at 22 °C. Excitation was at 330 nm, and panel B points represent the integrated intensity associated with the excimer emission peak centered near 480 nm.

maximal binding is observed at added peptide concentrations of about 60 nM for all three CaM-binding peptides to 100 nM CaM. These results suggest that the apparent dissociation constants of Py_2-CaM to these CaM-binding peptides are on the order of 10 nM. These values are consistent with prior measurements of the binding affinity of wild-type CaM to these CaM-binding peptides (*18, 19*), indicating that the pyrene labels do not interfere with normal binding. Similar binding affinities, ranging from 3 to 17 nM, have been reported between CaM and intact myosin light chain kinase, Ca-ATPase, and RyR1 proteins (*18*−*20*). These results, in total, suggest that the CaM-binding sequences of the Ca-ATPase or RyR calcium release channel represent a primary determinant in promoting the association with CaM for these target proteins.

There are substantial differences in the structures of bound CaM, as indicated by a 4-fold larger amount of excimer fluorescence observed for Py_2-CaM bound to either the C28W or the MLCK sequence as compared to RyR1 (Figure 2A); these results suggest a closer structural coupling between N- and C-terminal CaM domains in the former complexes. As excimer formation is an all-or-none phenomena requiring a close proximity between bound pyrenes; the lower excimer fluorescence of Py_2-CaM bound to RyRp suggests its increased spatial separation between N- and C-domains. In this complex, structural disorder promotes transient interactions between the opposing domains of CaM. This hypothesis is consistent with (i) the crystal structure of CaM bound to RyRp that shows a more extended conformation in comparison with that of MLCK (Figure 1) and (ii) the observation that the individual domains of CaM bound to the CaM-binding sequence of RyR1 are not strongly coupled to one another (*8*).

Dynamic Structural Differences between CaM-Binding Sequences of Ca-ATPase and RyR1. Prior measurements have demonstrated that a conserved Trp within CaM-binding peptides functions as a hydrophobic anchor that promotes the ordered binding of the opposing domains of CaM necessary for the CaM-dependent regulation of RyR1, the Ca-ATPase, and many other proteins (*1, 19, 21*). The absence of Trp side chains within the sequence of CaM permits measurements of changes in the dynamics of this conserved Trp to investigate structural characteristics of these CaM-binding sequences. We have, therefore, measured fluorescence lifetimes and rotational dynamics of the endogenous Trp within each CaM-binding peptide using frequency-domain fluorescence spectroscopy prior to and following CaM association.

Best fits to the lifetime data for either RyRp or C28W (donor only) require inclusion of three lifetime components, as indicated by the associated random residuals (Figures 3 and 4). Irrespective of CaM binding, the mean lifetime ($\bar{\tau}$) is substantially shorter for RyRp (1.2 ± 0.1 ns) in comparison to C28W (1.7 ± 0.2 ns), consistent with the high charge density proximal to the Trp side chains in RyRp in comparison to C28W. The differential phase and modulated anisotropies of the individual Trp side chains in RyRp and C28W were measured to assess their rotational dynamics (Figure 5). Because of its shorter lifetime, the modulated anisotropy is substantially larger for RyRp than C28W both before and after CaM binding. Increases in the differential phase for RyRp in comparison with C28W above 50 MHz are indicative of increased librational motion associated with the Trp side chain, which may arise as a result of contact interaction between the Trp side chain with the proximal Phe side chain in C28W, which is not present in RyRp. Thus, these time-resolved measurements of both fluorescence lifetimes and anisotropy are sensitive to local differences in environment of the conserved Trp in both peptides.

Prior to CaM binding, the frequency-response of the differential phase and modulated anistropy of either peptide are adequately described by two rotational correlation times, as indicated by the essentially random residuals. The shorter subnanosecond rotational correlation time (φ_1) corresponds to the independent librational mobility of the Trp side chain, while the longer rotational correlation time provides a measure of the overall hydrodynamic structure of the peptide. A consideration of the error surfaces of each fitting parameter indicates that the overall dynamics of RyRp and C28W is very similar prior to CaM binding, albeit with a diminished

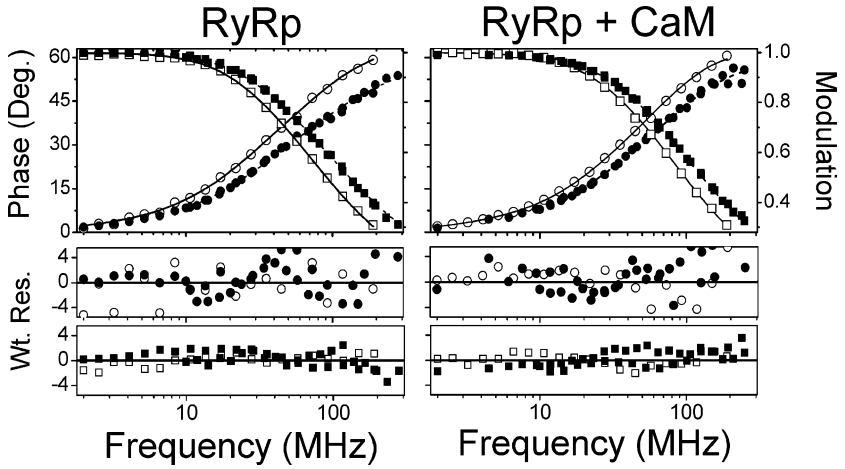

FIGURE 3: Effect of CaM binding on dimensions of CaM-binding sequence RyRp in RyR1. The frequency-response of the phase shift (○, ●) and modulation (□, ■) for the Trp^1 donor in the absence (○, □) and presence (●, ■) of the FRET acceptor 5-dimethylaminonaphthalene-1-sulfonyl (dansyl) covalently bound at Lys^{25} within the CaM-binding sequence of RyR1 (i.e., RyRp). Lines represent least-squares fit to a sum of exponentials (solid lines; ○, □) or to a Gaussian distribution of distances (dashed lines; ●, ■). Weighted residuals correspond to the difference between the experimental data and the fit normalized by the experimental error associated with the phase ($\delta_{phase} = 0.2°$) and modulation (i.e., $\delta_{mod} = 0.005$). Measurements were made in 10 mM HEPES (pH 7.4), 0.1 M KCl, 0.1 mM EGTA, and 190 μM $CaCl_2$ (100 μM free calcium) at 25 °C using 7.3 μM CaM and 5.7 μM RyRp. Excitation of Trp used the 297 nm line from the tripled output of a Ti-Sapphire laser (Coherent, Santa Clara, CA), and fluorescence emission was detected subsequent to a 350 nm interference filter using a K2 frequency-domain flourometer (ISS, Champaign, IL).

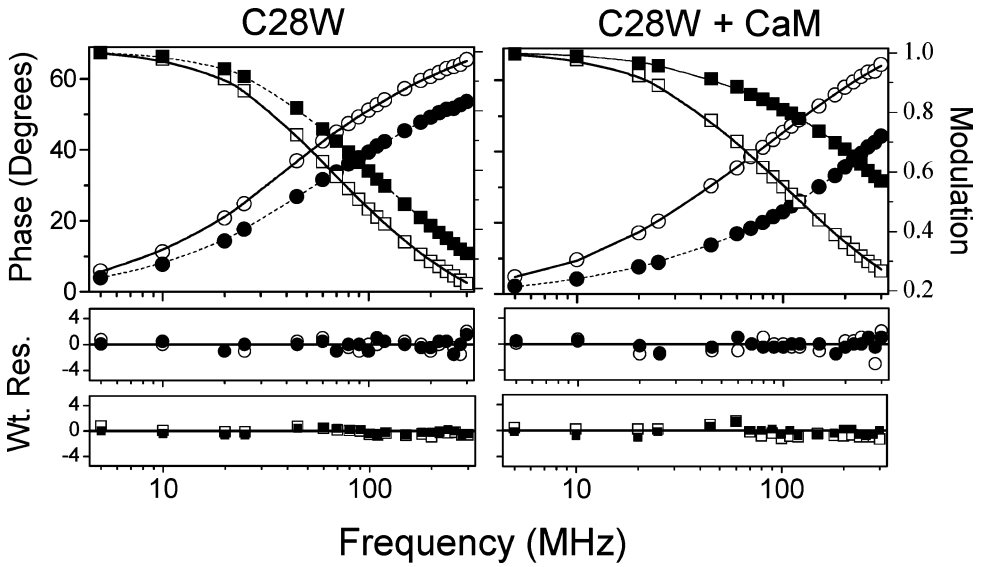

FIGURE 4: Effect of CaM binding on dimensions of CaM-binding sequence (C28W) peptide from Ca-ATPase. The frequency-response of the phase shift (○, ●) and modulation (□, ■) for the Trp^1 donor in the absence (○, □) and presence (●, ■) of the FRET acceptor AEDANS covalently bound at V14C within the CaM-binding sequence of the Ca-ATPase (i.e., C28W). Lines represent least-squares fit to a sum of exponentials (solid lines; ○, □) or to a Gaussian distribution of distances (dashed lines; ●, ■). Weighted residuals correspond to the difference between the experimental data and the fit normalized by the experimental error associated with the phase ($\delta_{phase} = 0.2°$) and modulation (i.e., $\delta_{mod} = 0.005$). Measurements were made in 100 mM HEPES (pH 7.5), 0.1 M KCl, and 100 μM $CaCl_2$ at 25 °C using 2.6 μM CaM and 2 μM C28W. Excitation of Trp was achieved using the 297 nm line from the tripled output of a Ti-Sapphire laser (Coherent, Santa Clara, CA), and fluorescence emission was detected subsequent to a 340 nm interference filter (bandwidth = 10 nm) using a K2 frequency-domain flourometer (ISS, Champaign, IL).

rate (longer correlation time) of side chain motion (φ_1) for C28W (Figure 6).

Upon CaM binding, there are substantial decreases in the rotational dynamics of the Trp side chain in both RyRp and C28W, as evidenced by the large increase in the modulated anisotropy and decrease in the differential phase for both RyRp and C28W (Figure 6). These decreases in rotational mobility are consistent with the suggested role of these Trp side chains in CaM binding (*1*). Fitting the data indicates that a single rotational correlation time ($\varphi \approx 7$ ns), associated with the overall hydrodynamic volume of the bound complex, is adequate to fully describe the data for CaM bound to C28W. The absence of independent Trp side chain mobility for C28W is consistent with the extensive van der Waals contacts apparent in the crystal structure of the C-domain of CaM bound to the Trp side chain (1cff).

The rotational correlation time for C28W bound to CaM is similar to previous measurements of this complex (*5*) and indicates a collapsed structure with a reduced hydrodynamic volume similar to that of CaM bound to the CaM-binding sequence in MLCK. In contrast, the rotational correlation time associated with the overall hydrodynamic volume for

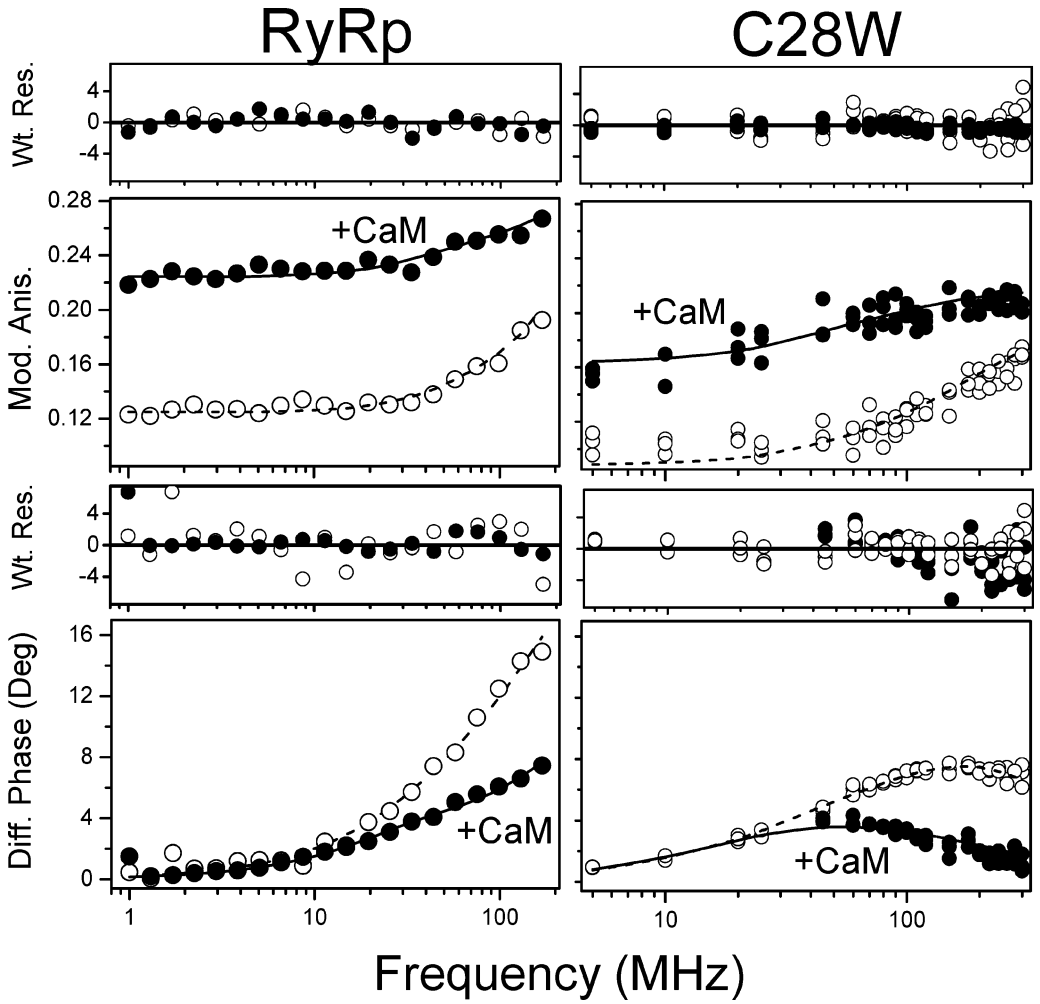

FIGURE 5: Reductions in Trp rotational mobility of RyRp and C28W upon CaM binding. Modulated anisotropy (top panels) and differential phase (bottom panels) data and associated nonlinear least-squares fits for Trp^1 in RyRp (left panels) or C28W (right panels) for CaM-binding peptide alone (○) and following association with CaM (●). Weighted residuals (wt res.) are shown above each plot and represent the difference between the experimental and the calculated values normalized by the errors for these respective measurements, which are 0.2° for the differential phase and 0.02 for the modulated anistropy. Experimental conditions are as described in the captions to Figures 4 and 5.

RyRp bound to CaM ($\varphi \approx 19$ ns) is substantially longer than that measured for C28W ($\varphi \approx 7$ ns). These results indicate a substantially larger overall hydrodynamic volume involving an extended structure for RyRp bound to CaM in comparison with either the RyRp peptide alone or the complex between C28W and CaM. Further, the correlation time for CaM bound to RyRp ($\varphi \approx 19$ ns) is substantially larger than that calculated from the crystal structure using the program HYDROPRO ($\varphi = 13.3$ ns) (*22*). These latter results suggest that the CaM-binding sequence is partially unstructured when bound to CaM. This latter observation is consistent with that of MacKenzie and co-workers, who demonstrated the presence of considerable flexibility in the complex between CaM and RyRp in solution, despite the appearance of an extended 22 amino acid helix in the crystal structure (*8*).

Large Differences in Conformational Heterogeneity of CaM-Binding Sequences. Crystal structures of CaM in complex with a wide range of CaM-binding sequences suggest that CaM commonly stabilizes the α-helical secondary structure within CaM-binding sequences to modulate protein function (see Figure S1 in the Supporting Information). In the case of RyR1, there remains considerable conformational flexibility in the solution structure of the complex between CaM and RyRp, despite the appearance of an extended helix in the high-resolution crystal structure (*8*). These latter results suggest that the determination of the structural disorder of CaM-binding sequences in complex with CaM may provide additional insight into the nature of target protein regulation. Accordingly, we have determined the conformational heterogeneity of the CaM-binding sequences from RyR1 or the Ca-ATPase through measurements of spatial separation using fluorescence resonance energy transfer (FRET). These measurements take advantage of the endogenous Trp donor and an appended acceptor chromophore incorporated during peptide synthesis to ensure complete labeling.

In comparison with the unlabeled peptide (donor only), there is a shift in the frequency-response of the phase shift and modulation to higher frequencies for both RyRp and C28W (Figures 3 and 4), indicating the presence of FRET. Prior to CaM binding, there is a relatively small (20−30 MHz) shift in the frequency-response of the lifetime data that is very similar for both RyRp and C28W, which is consistent with the expectation that both peptides are intrinsically unstructured. Upon CaM binding to RyRp, the

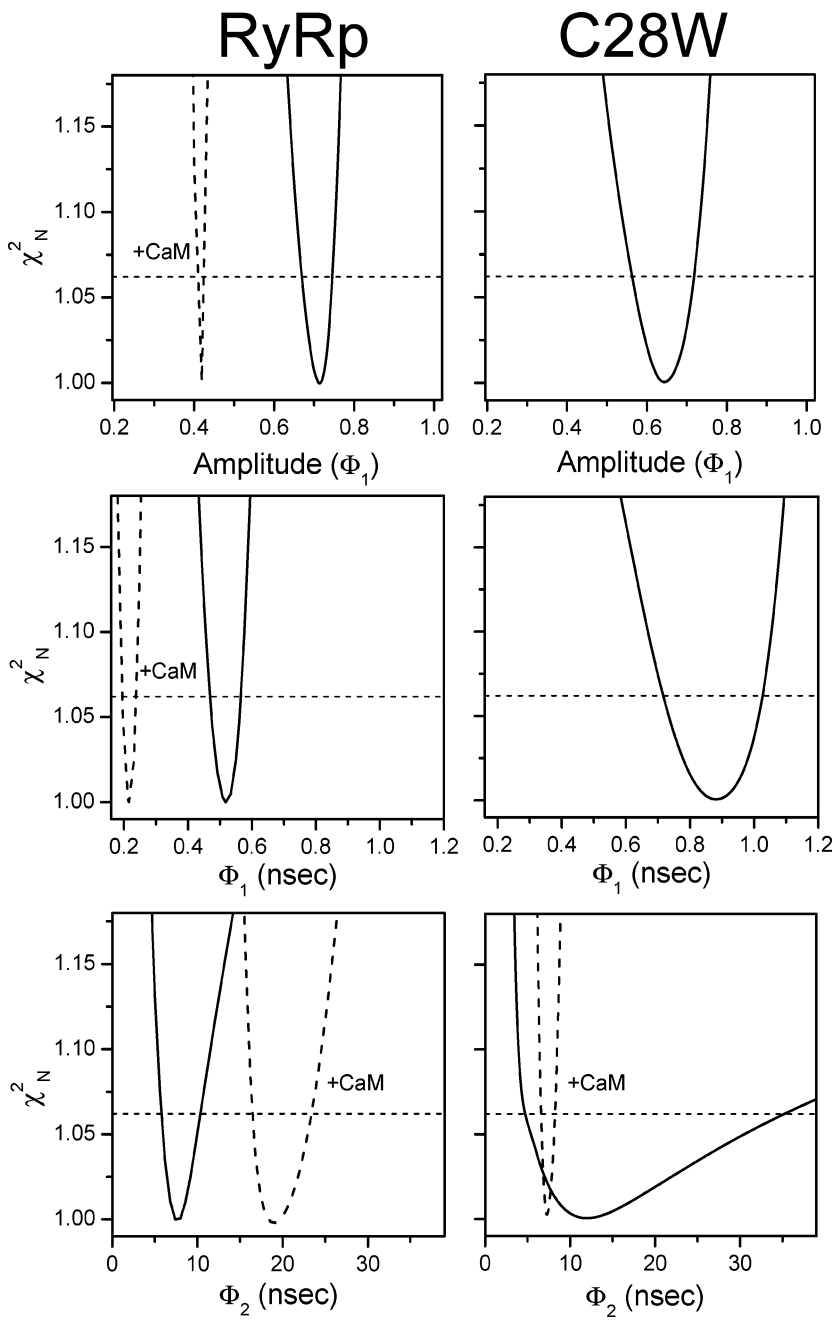

FIGURE 6: Compact or elongated hydrodynamic sizes of complexes between CaM and binding sequences from either RyR1 or the Ca-ATPase. Error surfaces are shown for the rotational dynamics of CaM-binding peptides RyRp (left panels) and C28W (right panels) associated with amplitude and rates for segmental motion of Trp side chain (φ_1) and overall motion of complex (φ_2). Normalized chi-squared vlaues (χ^2_N) result from nonlinear least-squares fits following the incremental adjustment of the fitting parameter obtained from the data depicted in Figure 5 for CaM-binding peptide alone (solid line) and following CaM binding (dashed line). All other fitting parameters were allowed to vary. The horizontal line corresponds to the *F*-statistic for one standard deviation. In the case of the complex between CaM and C28W, a single correlation time ($\varphi = 7$ ns) fully describes the data (lower right panel).

shift in the frequency-response remains similar to that of the unbound peptide (Figure 3), indicating the retention of a large spatial separation between Trp donor and acceptor chromophores irrespective of CaM binding. In contrast, CaM binding to C28W results in a large increase in FRET that is apparent from the large increase in the shift in the frequency-response of the lifetime data (Figure 4). Together, these results indicate that the average structures of RyRp and C28W bound to CaM are very different from one another, where the substantially larger increase in FRET upon CaM binding to C28W indicates a more compact structure. In comparison, the minimal change in FRET upon CaM binding to RyRp indicates a retention of the relatively large spatial separation between chromophores. These results indicate distinct differences with respect to the overall structures of the CaM-binding sequences of Ca-ATPase and RyR1 following CaM association that may underlie differences in their mechanisms of functional regulation.

An analysis of the time-dependent decay of FRET permits a determination of the conformational heterogeneity of the RyRp and C28W peptides (*14*, *23*). We therefore used the frequency-domain intensity decays of Trp in the absence and presence of the FRET acceptor to determine the average distance (R_{av}) and the half-width (hw) of the distribution of

Table 1: Summary of Conformational Dynamics for CaM-Binding Peptides of RyR1 and Ca-ATPase[a]

	lifetime data		anisotropy data		
sample	R_{av} (Å)[b]	hw (Å)[b]	g_1[c]	φ_1 (ns)[c]	φ_2 (ns)[c]
RyRp alone	<9.0	>51	0.71 (0.67−0.74)	0.51 (0.47−0.56)	8 (6−10)
RyRp + CaM	19 (10−21)	22 (17−35)	0.42 (0.41−0.43)	0.22 (0.19−0.24)	19 (17−23)
C28W alone	12 (10−14)	27 (25−30)	0.64 (0.56−0.72)	0.9 (0.7−1.0)	12 (5−35)
C28W + CaM	18.4 (18.2−18.6)	4 (3−5)	NA[d]	NA[d]	7.3 (6.4−8.2)

[a] Lifetime and rotational dynamics of Trp^1 in CaM-binding sequences of RyR1 calcium release channel (i.e., RyRp) or the plasma membrane Ca-ATPase (C28W) prior to and following association with CaM. [b] Average donor−acceptor separation (R_{av}) and half-width (hw) of the Gaussian distribution of distances calculated from data in Figures 3 and 4, as described by eq 2 in the Experimental Procedures, where the Förster distances for RyRp and C28W were, respectively, 20.6 and 21.1 Å. [c] Rotational dynamics calculated from data in Figure 5 involving amplitudes (g_1) and rates (φ_1) of Trp side chain motion or overall rotational dynamics of peptides bound to CaM (φ_2). Uncertainties of indicated values were determined from error surfaces and are indicated in parentheses. [d] NA: not applicable.

intermolecular distances (Table 1). From a consideration of the error surfaces (Figure 7), it is apparent that prior to CaM binding, there is a broad distribution of distances for both RyRp (hw > 51 Å) and C28W (hw = 27 Å) that is consistent with prior expectations that these peptides are unstructured in solution. Upon CaM binding to C28W, there is a 6 Å increase in the average spatial separation of donor and acceptor chromophores and a large reduction in conformational heterogeneity (hw = 4 ± 1 Å) that is indicative of the formation of a well-defined and compact structure. Following CaM binding, there is sufficient rotational mobility for both donor (i.e., $P = 0.21 \pm 0.01$) and acceptor (i.e., $P = 0.104 \pm 0.002$) chromophores to permit accurate measurements of the spatial separation within the measured distance range with minimal errors arising from orientational effects associated with the mobilities of the chromophores (*23*−*25*). The average separation determined from these measurements (i.e., 18 Å) is consistent with a helical structure, where the expected donor−acceptor separation between the donor−acceptor chromophores separated by 13 amino acids is about 20 Å for an α-helix. In contrast, upon CaM binding to RyRp, there is a very small decrease in the extent of conformational heterogeneity (hw = 23 Å) and a modest increase in the average spatial separation (R_{av} = 19 Å). While indicative of some increase in secondary structure, these results clearly indicate that in marked contrast to that observed for the Ca-ATPase, RyRp retains a considerable amount of structural heterogeneity when bound to CaM, which is indicative of some element of non-helical structure.

DISCUSSION

Summary of Results. We observe large differences in the structural properties of the CaM-binding sequences of the plasma membrane Ca-ATPase and RyR1 calcium release channel following their association with calcium-activated CaM (Table 1). In the case of the Ca-ATPase, CaM binding results in a disorder-to-order structural transition within the CaM-binding sequence C28W, resulting in a compact (φ = 7.3 ns) (Figure 6) and rigid (hw = 4 Å) (Figure 7) complex involving the direct juxtaposition of the opposing domains of CaM (Figure 1). These characteristics, in combination with the measured average spatial separation between donor−acceptor chromophores (i.e., R_{av} = 18 Å), are indicative of a rigid α-helical structure whose expected spatial separation for a 13 amino acid helical separation is 20 Å. No independent Trp side chain motion is observed within the peptide following CaM binding (Figure 6), consistent with the key role of Trp as a hydrophobic anchor in mediating CaM binding (*1*). In comparison, for the CaM-binding sequence of RyR1, CaM binding stabilizes an elongated structure (φ_2 = 19 ns) with a significant spatial separation between the opposing domains of CaM (Figure 1). Moreover, the CaM-binding sequence of RyR1 adopts a heterogeneous range of conformers (hw = 22 Å) (Figure 7). Following CaM binding, the subnanosecond mobility of Trp is retained (albeit with a diminished amplitude) within the CaM-binding sequence of RyR1 (Figure 6). These latter results are consistent with the larger structural heterogeneity and absence of contact interactions between the opposing domains of CaM. The comparison of these CaM target complexes indicates an important role for interdomain contact interactions between the opposing domains of CaM in the stabilization of an extended and rigid helical sequence within the CaM-binding sequences of target proteins. Further, these results suggest a plasticity in how CaM modulates target protein function that is consistent with the known mechanisms underlying the CaM-dependent regulation of the Ca-ATPase and RyR1 calcium release channel (Figure 8).

Structures of CaM-Binding Sequences. Most binding interactions involving CaM and target proteins are calcium dependent. In the majority of available structures, the complex between calcium-activated CaM and CaM-binding sequences assumes a compact structure (see Figure S1 in the Supporting Information). The opposing domains of CaM wrap around the binding sequence to bring the opposing domains into close proximity, much as originally reported for the CaM-binding sequence of skeletal myosin light chain kinase (MLCK) (Figure 1) (*7*). Within this family of structures, distinct CaM-binding motifs are apparent based on the spacing of conserved hydrophobic side chains in target peptides, which contribute to differences in the spatial separation of the opposing domains of calcium-activated CaM bound to target peptides (*2*). An apparent exception to this mechanism of binding is the extended CaM structure observed in the high-resolution structure of the complex with a sequence of the plasma membrane Ca-ATPase (1cff). However, this structure involves only the binding sequence for the C-domain of CaM (i.e., C20W), whereas binding of both C- and N-domains of CaM to the full sequence (i.e., C28W) forms a compact structure similar to that of the

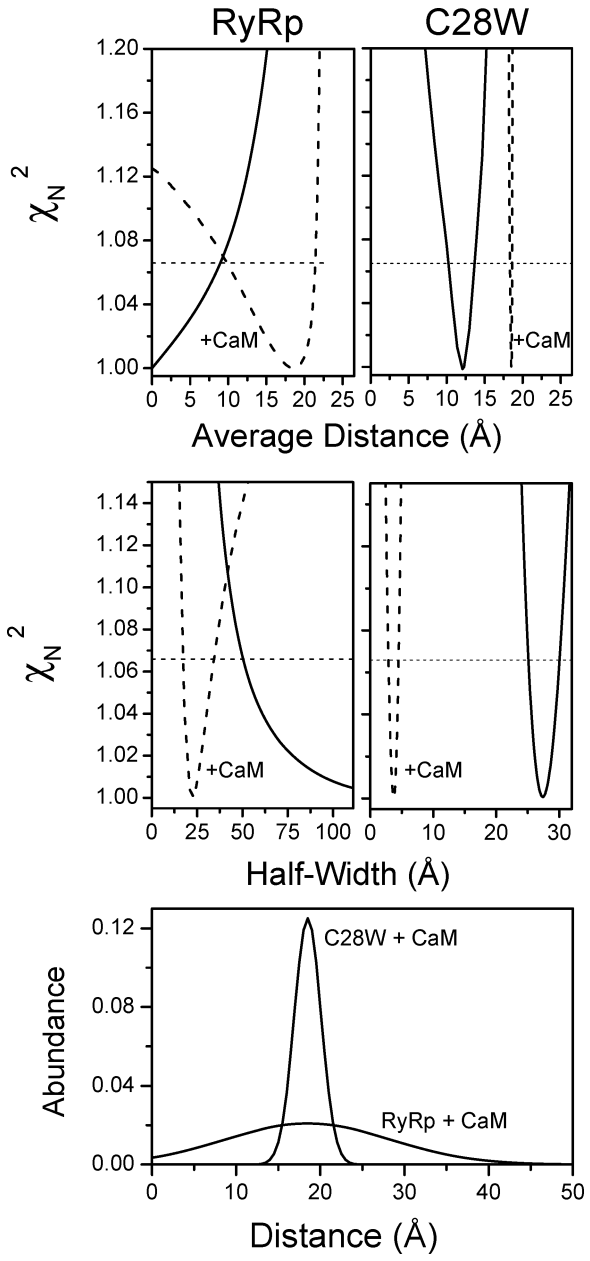

FIGURE 7: Conformational heterogeneity associated with CaM-binding sequences from FRET measurements. Representation of distance distributions for CaM-binding sequences from RyR1 (i.e., RyRp) and the Ca-ATPase (C28W) bound to CaM (bottom panel) and depiction of associated error surfaces for average distance (R_{av}) and half-widths of Gaussian distance distributions (top panels) for CaM-binding peptides RyRp or C28W alone (solid lines) and following CaM binding (dashed lines). Normalized chi-squared values (χ^2_N) result from nonlinear least-squares fits following the incremental adjustment of the fitting parameter obtained from the data depicted in Figures 3 and 4 for CaM-binding peptide RyRp and C28W alone (solid line) and following CaM binding (dashed line). All other fitting parameters were allowed to vary. The horizontal line corresponds to the *F*-statistic for one standard deviation.

MLCK complex that is necessary for enzyme activation (Figure 1) (*5*, *10*, *19*, *26*).

Another common class of CaM-binding proteins involves the calcium-independent binding between apo-CaM and target proteins, which commonly occur through IQ motifs (*2*, *27*). Additional novel binding motifs have been identified that involve extended conformations of CaM in association with multiple subunits in macromolecular target complexes and include anthrax adenylyl cyclase and the calcium gated potassium channel (*28*, *29*). These latter structures suggest a plasticity in binding interactions between CaM and different target proteins, which may involve either targeted structural changes within monomeric proteins (e.g., the Ca-ATPase) or the modulation of intersubunit interactions in supramolecular protein complexes (e.g., RyR1 calcium release channel). What has been unclear is the nature of the conformational switching and functional role of changes in the mode of CaM binding in these latter proteins that bind extended CaM structures.

CaM-Dependent Regulation of the Ca-ATPase. Prior measurements have measured the dissociation of the inhibitory domain of the Ca-ATPase upon association with CaM, which is necessary for enzyme activation (*4*, *30*, *31*). Further, post-translational modifications that induce disruption of contact interactions between the opposing domains of CaM are known to block the dissociation of the inhibitory domain and to result in a diminished activation of the Ca-ATPase (*30*, *32*−*35*). These latter results are consistent with the current measurements suggesting that contact interactions between the N- and the C-domains of CaM in complex with the CaM-binding sequence of the Ca-ATPase, with the associated stabilization of the helical structure of the target, act as a molecular switch that triggers the dissociation of the inhibitory domain necessary for Ca-ATPase enzyme activation (Figure 8).

CaM-Dependent Regulation of RyR1. Differences in binding interactions between apo- and calcium-activated CaM and noncontiguous CaM-binding sequences have been suggested to modulate channel activity through the modulation of intersubunit interactions in RyR1 as well as $Ca_v1.2$ channels (*8*, *36*−*38*). In both of these examples, available structures of calcium-activated CaM bound to high-affinity CaM-binding sequences indicate minimal contact interactions between N- and C-domains of CaM (*8*, *36*, *39*). Likewise, calcium-activated CaM is proposed to modulate intersubunit interactions in the cyclic nucleotide gated (CNG) channel (*40*), where CaM in complex with the CaM-binding sequence adopts a similar structure to that observed for RyR1 and $Ca_v1.2$ channels (see Figure S1 in the Supporting Information). The current results, which indicate that the high-affinity CaM-binding sequence of RyR1 (i.e., K^{3614}−K^{3643}) remains conformationally disordered upon CaM association, is consistent with a model in which the calcium-dependent loss of intersubunit interactions within the RyR1 tetramer is responsible for the inhibition of channel function (Figure 8B). In this model, CaM with two calcium ions bound in the C-terminal domain mediates intersubunit coupling to promote channel activation. This is consistent with prior suggestions that the C-terminus interacts with the high-affinity binding peptide K^{3614}−K^{3643} (*21*, *41*) and that the N-domain of apo-CaM interacts with a lower affinity CaM-binding sequence to modulate intersubunit interactions (i.e., S^{1975}−R^{1999}) (*6*, *8*, *37*). Calcium activation of the N-terminal domain results in high-affinity binding of both N- and C-domains of CaM to high-affinity binding peptide K^{3614}−K^{3643}, which acts to disrupt intersubunit interactions to promote channel inhibition.

General Principles Underlying the CaM-Dependent Regulation of Protein Function. The CaM-dependent regulation of the majority of target enzymes involves either the

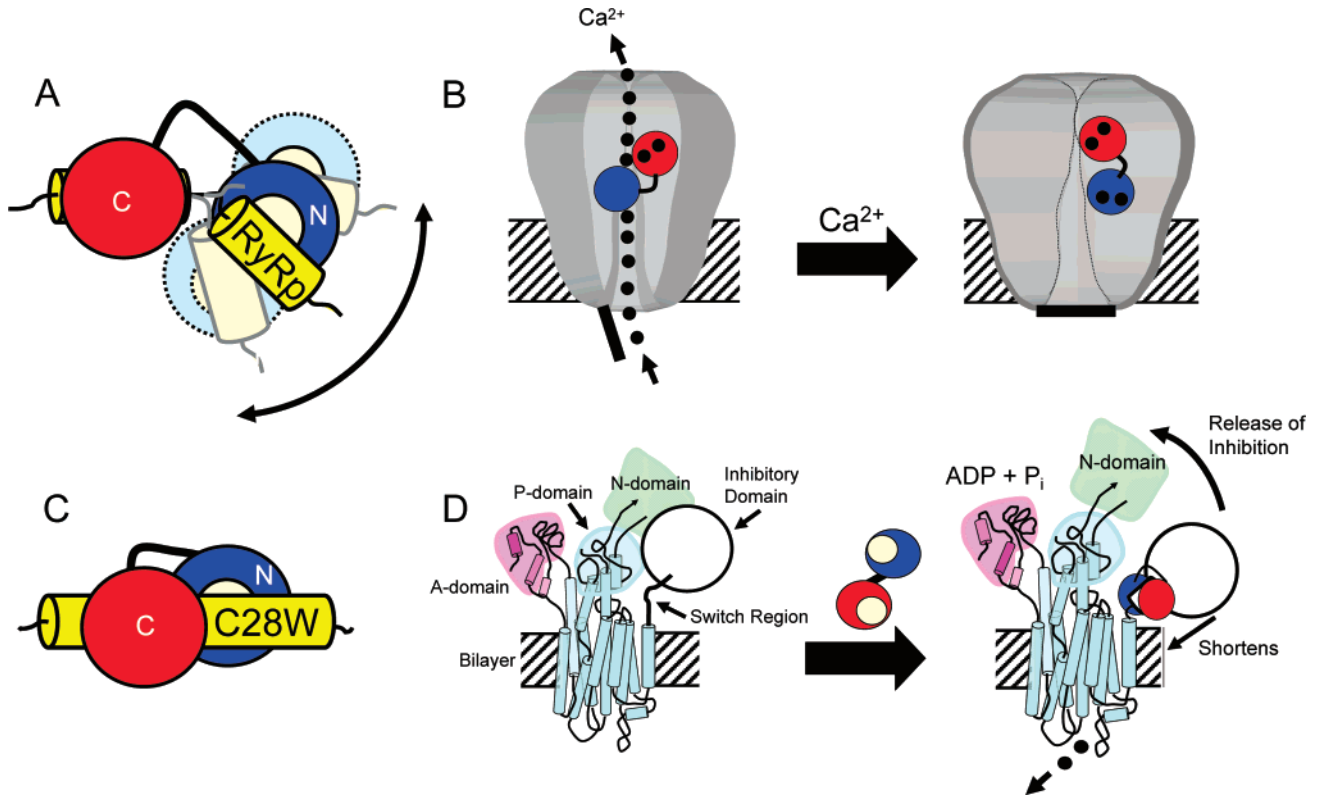

FIGURE 8: Stabilization of helical structure of binding sequence depends on contact interactions between N- and C-domains of CaM. Model depicting conformational heterogeneity within CaM-binding sequence RyRp (A) or structured helix in C28W (C) in complex with N- and C-domains of CaM (shown in blue and red) and proposed functional consequences associated with RyR1 channel inhibition (B) or Ca-ATPase enzymatic activation (D). Binding cleft in calcium-activated CaM is shown in yellow in panel D. In panel B, CaM with two calcium ions bound in the C-terminal domain, resulting in RyR1 channel activation, is shown mediating intersubunit coupling consistent with prior suggestions that the C-terminus interacts with the high-affinity binding peptide $K^{3614}-K^{3643}$ (*21*, *41*) and that the N-domain interacts with a lower affinity CaM-binding sequence to modulate intersubunit interactions (i.e., $S^{1975}-R^{1999}$) (*8*, *37*). Calcium activation of the N-terminal domain results in high-affinity binding of both N- and C-domains of CaM to $K^{3614}-K^{3643}$, which is suggested to result in the stabilization of an inhibited state through diminished intersubunit interactions (*6*). In panel D, calcium-activated CaM binds to the switch region of the Ca-ATPase, whose physical shortening upon the stabilization of the α-heliical structure is proposed to result in the dissociation of the inhibitory domain necessary for enzyme activation.

displacement of an inhibitory domain by fully calcium-activated CaM or the stabilization of protein−protein interactions necessary for optimal enzyme activity (*4*, *30*, *31*, *42*−*45*). Of the CaM-dependent enzymes that are activated upon CaM binding through the displacement of an inhibitory domain (e.g., plasma membrane Ca-ATPase, MLCK, or CaM-dependent protein kinase), available structures indicate a conserved mechanism involving a linear CaM-binding sequence that associates with CaM in a collapsed structure that brings the opposing domains of CaM into close proximity to stabilize an extended helical CaM-binding sequence (*46*). Structures of CaM bound to the intact protein and a peptide corresponding to the CaM-binding sequence are virtually identical for both CaM-dependent protein kinase I and Ca-ATPase (*3*−*5*). These latter results suggest that the formation of the collapsed structure of CaM and the associated stabilization of the secondary structure of the CaM-binding sequence are necessary for the dissociation of the regulatory domain necessary for target protein activation.

In contrast, the stabilization of activated oligomeric protein complexes commonly involves the simultaneous binding of the opposing domains of CaM to different CaM-binding sequences in a more extended structure (*44*). For example, the opposing domains of calcium-activated CaM each bind a separate binding peptide in glutamate decarboxylase (1nwd), which is suggested to stabilize the activated dimeric form of the enzyme (*45*). Calcium-activated CaM binds in an extended conformation to the multiple peptides corresponding to the CaM-binding sequence of calcineurin (2f2o), which has been suggested to represent a possible means to couple CaM-dependent proteins that contain multiple IQ motifs (*47*). Likewise, extended structures of partially calcium-activated CaM bound to anthrax adenylate cyclase (1yrt) or the calcium-gated potassium channel (1g4y) are suggested to modulate target protein function through the modulation of allosteric interactions between protein subunits in multiprotein complexes (*28*, *29*, *44*). In these examples, calcium-dependent changes in the binding of CaM to different sequences provide a means to modulate allosteric interactions within multiprotein complexes. For example, in the inactive conformation of myosin-5a, the C-domain of apo-CaM is unable to bind calcium ions due to the incorrect orientation of several residues involved in chelation (*48*). Calcium binding serves as a trigger to modulate CaM binding to target sequences to induce motility, providing a means to rapidly modulate enzyme activity in response to calcium binding. Similar conformations of CaM with associated changes in target protein binding are likely to serve as a general mechanism to modulate target protein function.

Conclusions and Future Directions. CaM interdomain associations upon complexation with CaM-binding sequences can function as part of a conformational switching mecha-

nism to modulate structure and dynamics. Contact interactions between the opposing domains of CaM in association with the CaM-binding sequence of the Ca-ATPase utilize domain−domain interactions to form a rigid structural complex whose overall dimensions are reduced, thus acting as a structural switch that induces the release of the inhibitory domain necessary for enzyme activation (Figure 8D). In contrast, in the absence of CaM interdomain interactions, the CaM-RyRp complex is a conformationally flexible structure. The retention of a conformationally flexible CaM-binding sequence may facilitate the association between both N- and C-domains of CaM to permit the release of intersubunit interactions within the RyR1 tetramer associated with channel activation (Figure 8B). Future measurements are needed to directly assess the conformation and dynamics of CaM-binding sequences in target proteins prior to and following CaM binding, and their relationship to possible domain reorientations associated with target protein enzymatic regulation, permitting direct comparisons of structure and function. These latter measurements should directly assess possible secondary interactions between CaM and regions of target proteins not directly associated with the binding interface, which have previously been shown to have the potential to regulate the function of myosin light chain kinase (*49*).

SUPPORTING INFORMATION AVAILABLE

Known structures between CaM and CaM-binding sequences from 20 target proteins (Figure S1). This material is available free of charge via the Internet at http://pubs.acs.org.

REFERENCES

1. Crivici, A., and Ikura, M. (1995) Molecular and structural basis of target recognition by calmodulin, *Annu. Rev. Biophys. Biomol. Struct. 24*, 85−116.
2. Rhoads, A. R., and Friedberg, F. (1997) Sequence motifs for calmodulin recognition, *FASEB J. 11*, 331−340.
3. Kranz, J. K., Lee, E. K., Nairn, A. C., and Wand, A. J. (2002) A direct test of the reductionist approach to structural studies of calmodulin activity: Relevance of peptide models of target proteins, *J. Biol. Chem. 277*, 16351−16354.
4. Yao, Y., Gao, J., and Squier, T. C. (1996) Dynamic structure of the calmodulin-binding domain of the plasma membrane Ca-ATPase in native erythrocyte ghost membranes, *Biochemistry 35*, 12015−12028.
5. Yao, Y., and Squier, T. C. (1996) Variable conformation and dynamics of calmodulin complexed with peptides derived from the autoinhibitory domains of target proteins, *Biochemistry 35*, 6815−6827.
6. Boschek, C., Jones, T., Squier, T. C., and Bigelow, D. J. (2007) Calcium occupancy of N-terminal sites within calmodulin induces inhibition of RyR1 calcium release channel, *Biochemistry 46*, 10621−10628.
7. Ikura, M., Barbato, G., Klee, C. B., and Bax, A. (1992) Solution structure of calmodulin and its complex with a myosin light chain kinase fragment, *Cell Calcium 13*, 391−400.
8. Maximciuc, A. A., Putkey, J. A., Shamoo, Y., and MacKenzie, K. R. (2006) Complex of calmodulin with a ryanodine receptor target reveals a novel, flexible binding mode, *Structure 14*, 1547−1556.
9. Boschek, C. B., Squier, T. C., and Bigelow, D. J. (2007) Disruption of interdomain interactions via partial calcium occupancy of calmodulin, *Biochemistry 46*, 4580−4588.
10. Elshorst, B., Hennig, M., Forsterling, H., Diener, A., Maurer, M., Schulte, P., Schwalbe, H., Griesinger, C., Krebs, J., Schmid, H., Vorherr, T., and Carafoli, E. (1999) NMR solution structure of a complex of calmodulin with a binding peptide of the Ca^{2+} pump, *Biochemistry 38*, 12320−12332.
11. Strasburg, G. M., Hogan, M., Birmachu, W., Thomas, D. D., and Louis, C. F. (1988) Site-specific derivatives of wheat germ calmodulin. Interactions with troponin and sarcoplasmic reticulum, *J. Biol. Chem. 263*, 542−548.
12. Haugland, R. E. (2002) *Handbook of Fluorescent Probes and Research Products*, Molecular Probes, Inc., Eugene, OR.
13. Lakowicz, J. R., and Gryczynski, I. (1991) Frequency-Domain Fluorescence Spectroscopy, in *Topics in Fluorescence Spectropscopy* (Lakowicz, J. R., Ed.) Vol. 1, pp 293−335, Plenum Press, New York.
14. Cheung, H. C. (1991) Resonance Energy Transfer, in *Topics in Fluorescence Spectroscopy* (Lakowicz, J. R., Ed.) Vol. 2, pp 128−176, Plenum Press, New York.
15. Lehrer, S. S. (1997) Intramolecular pyrene excimer fluorescence: A probe of proximity and protein conformational change, *Methods Enzymol. 278*, 286−295.
16. Project, E., Friedman, R., Nachliel, E., and Gutman, M. (2006) A molecular dynamics study of the effect of Ca^{2+} removal on calmodulin structure, *Biophys. J. 90*, 3842−3850.
17. Qin, Z., and Squier, T. C. (2001) Calcium-dependent stabilization of the central sequence between Met(76) and Ser(81) in vertebrate calmodulin, *Biophys. J. 81*, 2908−2918.
18. Rodney, G. G., Moore, C. P., Williams, B. Y., Zhang, J. Z., Krol, J., Pedersen, S. E., and Hamilton, S. L. (2001) Calcium binding to calmodulin leads to an N-terminal shift in its binding site on the ryanodine receptor, *J. Biol. Chem. 276*, 2069−2074.
19. Sun, H., and Squier, T. C. (2000) Ordered and cooperative binding of opposing globular domains of calmodulin to the plasma membrane Ca-ATPase, *J. Biol. Chem. 275*, 1731−1738.
20. Quadroni, M., L'Hostis, E. L., Corti, C., Myagkikh, I., Durussel, I., Cox, J., James, P., and Carafoli, E. (1998) Phosphorylation of calmodulin alters its potency as an activator of target enzymes, *Biochemistry 37*, 6523−6532.
21. Yamaguchi, N., Xin, C., and Meissner, G. (2001) Identification of apocalmodulin and Ca^{2+}-calmodulin regulatory domain in skeletal muscle Ca^{2+} release channel, ryanodine receptor, *J. Biol. Chem. 276*, 22579−22585.
22. Garcia De La Torre, J., Huertas, M. L., and Carrasco, B. (2000) Calculation of hydrodynamic properties of globular proteins from their atomic-level structure, *Biophys. J. 78*, 719−730.
23. Haas, E., Katchalski-Katzir, E., and Steinberg, I. Z. (1978) Effect of the orientation of donor and acceptor on the probability of energy transfer involving electronic transitions of mixed polarization, *Biochemistry 17*, 5064−5070.
24. Wu, P., and Brand, L. (1992) Orientation factor in steady-state and time-resolved resonance energy transfer measurements, *Biochemistry 31*, 7939−7947.
25. Dale, R. E., and Eisinger, J. (1976) Intramolecular energy transfer and molecular conformation, *Proc. Natl. Acad. Sci. U.S.A. 73*, 271−273.
26. Anbanandam, A., Bieber Urbauer, R. J., Bartlett, R. K., Smallwood, H. S., Squier, T. C., and Urbauer, J. L. (2005) Mediating molecular recognition by methionine oxidation: Conformational switching by oxidation of methionine in the carboxyl-terminal domain of calmodulin, *Biochemistry 44*, 9486−9496.
27. Bahler, M., and Rhoads, A. (2002) Calmodulin signaling via the IQ motif, *FEBS Lett. 513*, 107−113.
28. Drum, C. L., Yan, S. Z., Bard, J., Shen, Y. Q., Lu, D., Soelaiman, S., Grabarek, Z., Bohm, A., and Tang, W. J. (2002) Structural basis for the activation of anthrax adenylyl cyclase exotoxin by calmodulin, *Nature (London, U.K.) 415*, 396−402.
29. Schumacher, M. A., Rivard, A. F., Bachinger, H. P., and Adelman, J. P. (2001) Structure of the gating domain of a Ca^{2+}-activated K^+ channel complexed with Ca^{2+}/calmodulin, *Nature (London, U.K.) 410*, 1120−1124.
30. Osborn, K. D., Bartlett, R. K., Mandal, A., Zaidi, A., Urbauer, R. J., Urbauer, J. L., Galeva, N., Williams, T. D., and Johnson, C. K. (2004) Single-molecule dynamics reveal an altered conformation for the autoinhibitory domain of plasma membrane Ca($^{2+}$)-ATPase bound to oxidatively modified calmodulin, *Biochemistry 43*, 12937−12944.
31. Osborn, K. D., Zaidi, A., Mandal, A., Urbauer, R. J., and Johnson, C. K. (2004) Single-molecule dynamics of the calcium-dependent activation of plasma-membrane Ca^{2+}-ATPase by calmodulin, *Biophys. J. 87*, 1892−1899.
32. Bartlett, R. K., Bieber Urbauer, R. J., Anbanandam, A., Smallwood, H. S., Urbauer, J. L., and Squier, T. C. (2003) Oxidation

of Met144 and Met145 in calmodulin blocks calmodulin dependent activation of the plasma membrane Ca-ATPase, *Biochemistry 42*, 3231−3238.
33. Boschek, C. B., Jones, T., Smallwood, H. S., Squier, T. C., and Bigelow, D. J. (2008) Loss of the calmodulin-dependent inhibition of RyR1 calcium release channel upon oxidaiton of methionines in calmodulin, *Biochemistry 47*, 131−142.
34. Yao, Y., Yin, D., Jas, G. S., Kuczer, K., Williams, T. D., Schoneich, C., and Squier, T. C. (1996) Oxidative modification of a carboxyl-terminal vicinal methionine in calmodulin by hydrogen peroxide inhibits calmodulin-dependent activation of the plasma membrane Ca-ATPase, *Biochemistry 35*, 2767−2787.
35. Yin, D., Kuczera, K., and Squier, T. C. (2000) The sensitivity of carboxyl-terminal methionines in calmodulin isoforms to oxidation by H(2)O(2) modulates the ability to activate the plasma membrane Ca-ATPase, *Chem. Res. Toxicol. 13*, 103−110.
36. Fallon, J. L., Halling, D. B., Hamilton, S. L., and Quiocho, F. A. (2005) Structure of calmodulin bound to the hydrophobic IQ domain of the cardiac Ca(v)1.2 calcium channel, *Structure 13*, 1881−1886.
37. Zhang, H., Zhang, J. Z., Danila, C. I., and Hamilton, S. L. (2003) A noncontiguous, intersubunit binding site for calmodulin on the skeletal muscle Ca^{2+} release channel, *J. Biol. Chem. 278*, 8348−8355.
38. Kobayashi, T., Yamada, Y., Fukao, M., Tsutsuura, M., and Tohse, N. (2007) Regulation of Cav1.2 current: Interaction with intracellular molecules, *J. Pharmacol. Sci. 103*, 347−353.
39. Van Petegem, F., Chatelain, F. C., and Minor, D. L., Jr. (2005) Insights into voltage-gated calcium channel regulation from the structure of the CaV1.2 IQ domain-Ca^{2+}/calmodulin complex, *Nat. Struct. Mol. Biol. 12*, 1108−1115.
40. Contessa, G. M., Orsale, M., Melino, S., Torre, V., Paci, M., Desideri, A., and Cicero, D. O. (2005) Structure of calmodulin complexed with an olfactory CNG channel fragment and role of the central linker: Residual dipolar couplings to evaluate calmodulin binding modes outside the kinase family, *J. Biomol. NMR 31*, 185−199.
41. Moore, C. P., Rodney, G., Zhang, J. Z., Santacruz-Toloza, L., Strasburg, G., and Hamilton, S. L. (1999) Apocalmodulin and Ca^{2+} calmodulin bind to the same region on the skeletal muscle Ca^{2+} release channel, *Biochemistry 38*, 8532−8537.
42. Goldberg, J., Nairn, A. C., and Kuriyan, J. (1996) Structural basis for the autoinhibition of calcium/calmodulin-dependent protein kinase I, *Cell 84*, 875−887.
43. Heller, W. T., Krueger, J. K., and Trewhella, J. (2003) Further insights into calmodulin-myosin light chain kinase interaction from solution scattering and shape restoration, *Biochemistry 42*, 10579−10588.
44. Vetter, S. W., and Leclerc, E. (2003) Novel aspects of calmodulin target recognition and activation, *Eur. J. Biochem. 270*, 404−414.
45. Yap, K. L., Yuan, T., Mal, T. K., Vogel, H. J., and Ikura, M. (2003) Structural basis for simultaneous binding of two carboxy-terminal peptides of plant glutamate decarboxylase to calmodulin, *J. Mol. Biol. 328*, 193−204.
46. Hoeflich, K., and Ikura, M. (2002) Calmodulin in action: Diversity in target recognition and activation mechanisms, *Cell Calcium 108*, 739−742.
47. Ye, Q., Li, X., Wong, A., Wei, Q., and Jia, Z. (2006) Structure of calmodulin bound to a calcineurin peptide: A new way of making an old binding mode, *Biochemistry 45*, 738−745.
48. Houdusse, A., Gaucher, J. F., Krementsova, E., Mui, S., Trybus, K. M., and Cohen, C. (2006) Crystal structure of apo-calmodulin bound to the first two IQ motifs of myosin V reveals essential recognition features, *Proc. Natl. Acad. Sci. U.S.A. 103*, 19326−19331.
49. Persechini, A., Gansz, K. J., and Paresi, R. J. (1996) A role in enzyme activation for the N-terminal leader sequence in calmodulin, *J. Biol. Chem. 271*, 19279−19282.
50. Humphrey, W., Dalke, A., and Schulten, K. (1996) VMD: Visual molecular dynamics, *J. Mol. Graphics 14*, 27−38.

BI701987N